Comparison of Wide-Area and Local Power Oscillation Damping Control Through Inverter-Based Resources

Yi Zhao[1], Khaled Mohammed Alshuaibi[1], Xinlan Jia[1], Chengwen Zhang[1], Yilu Liu[1,2]
1. The University of Tennessee, Knoxville, TN, USA
2. Oak Ridge National Laboratory, Oak Ridge, TN, USA
{yzhao77, liu}@utk.edu

Deepak Ramasubramanian[3], Lin Zhu[3], Evangelos Farantatos[3]
3. Electric Power Research Institute, Palo Alto, CA, USA
{dramasubramanian, lzhu, efarantatos}@epri.com

***Abstract*—Power System Stabilizers (PSSs) at conventional synchronous generators have proved to be effective in suppressing both local and inter-area low-frequency oscillations (LFOs). However, the retirement of conventional synchronous generators and the increasing penetration of inverter-based resources (IBRs) can potentially lead to insufficient stabilizing capability available from the remaining conventional synchronous generators. In this paper, the control performance of Power Oscillation Damping (POD) through IBRs with either wide-area measurements or local measurements as an input signal is investigated. The performance of IBR based POD control is also compared with wide-area POD control via synchronous generators. Case studies are carried out on a synthetic Texas power system model. Simulation results demonstrate that the proposed POD through active power modulation of IBRs is more effective than POD through reactive power modulation of IBRs and wide-area POD via synchronous generators. The proposed POD can be supplementary to the PSSs at conventional synchronous generators for power grids with high renewable penetration.**

***Index Terms*— Inverter-based resources (IBRs), low-frequency oscillation, measurement-driven model, phasor measurement unit (PMU), power oscillation damping (POD).**

I. INTRODUCTION

Power System Stabilizers (PSSs) at conventional synchronous generators are commonly used to suppress low-frequency oscillations (LFOs) in large-scale power systems [1-2]. The retirement of conventional synchronous generators and the increasing integration of inverter-based renewable resources (IBRs) will further aggravate the stability of LFOs and reduce the stabilizing capability of LFOs from the remaining conventional generators [3]. Moreover, the remaining conventional synchronous generators may be located at areas that lack sufficient controllability to suppress the LFOs.

Meanwhile, IBRs are displacing conventional synchronous generators resulting in high renewable penetration power grids and become the dominant resources that can provide fast oscillation damping control of LFOs [4-5]. Different from synchronous generators, POD control at IBRs can be designed to suppress the LFO either by modulating the active or reactive power of IBRs. To avoid destabilizing other modes of oscillation and generating new forms of stability issues, PODs at IBRs must be accurately designed and tuned. A sufficient damping of LFOs with POD control applied at the IBRs is extremely vital to the future power system.

Considering that wide-area measurements from phasor measurement units (PMUs) are more effective in damping LFOs than local signals, PODs with the use of wide-area feedback signals at synchronous generators, energy storage and HVDCs [6-8] have been widely investigated. However, many POD designing methods for IBRs [9-10] are still highly dependent on the grid simulation model accuracy. Due to the dramatic variations of renewables and load demand, the power grid dynamic properties will change significantly and are difficult to be modeled accurately in real-time.

To ensure the POD performance through IBRs, this paper proposes a comprehensive POD design procedure at IBRs, including the optimal feedback signal selection and IBR actuator selection for PODs, a measurement-driven method to depict the system oscillatory dynamics, and POD parameter calculation method. Different from other physical model-based POD design method, this measurement-driven method predicts the system oscillation dynamics using a simplified linear transfer function model built online with real-time measurements. This proposed POD controller at IBRs can avoid the power system model accuracy impact and guarantee its damping performance in real time.

The rest of this paper is organized as follows. Section II provides the structure of power system with POD through IBR. Section III introduces an overview of the proposed POD design procedure and the details of POD design method. The synthetic Texas power system case study with PODs at IBRs is presented in Section IV. Section V concludes this paper.

II. POWER OSCILLATION DAMPING CONTROL SYSTEM

A. *Power System with POD Through IBR*

The block diagram of a power system with POD through

This work was primarily supported by Electric Power Research Institute (EPRI) and partly supported by National Science Foundation under the Award Number 1839684 and 1941101. This work also made use of Engineering Research Center Shared Facilities supported by the Engineering Research Center Program of the National Science Foundation and DOE under NSF Award Number EEC-1041877 and the CURENT Industry Partnership Program.

an IBR is shown in Fig. 1. Δf is the observation signal for the POD which can be collected from remote PMUs or the local IBR bus. The IBR receives the output of the POD and adjusts its active power output or reactive power output to damp the oscillations in the system. The electrical model of the IBR in this study consists of converter model (REGCAU2) and electrical control model (REECCU1) which are developed under the Western Electricity Coordinating Council (WECC) Renewable Energy Modeling Task Force [11]. The active power control command from POD is added as an auxiliary signal (*Paux*) of the REECCU1 model to modulate the active current command of the IBR. Reactive power control command from the POD is added to *pfaref* to modulate the power factor of the IBR. The power factor flag (*PfFlag*), voltage control flag (*VFlag*), and reactive power control flag (*QFlag*) are set to be 1 to ensure the reactive power modulation through the IBR.

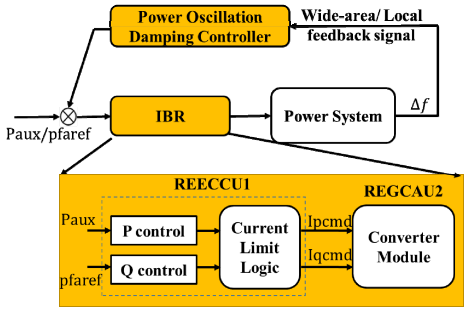

Figure 1. Power system with POD through IBRs

B. *POD Structure*

The POD controller is based on the lead-lag structure, which consists of a washout block, a filter, two phase compensation blocks, a gain block, and a rate limiter [12]. Fig. 2 illustrates the block diagram of the POD controller. Rate limiter is set to be 1 p.u./ s to prevent the rapid change of active or reactive power modulation of the IBR. The time constant T_w of the washout block is 10s. The transfer function of the band-pass filter in Fig. 2 is [13]:

$$K_f(s) = (\omega_k s / Q) / (s^2 + \omega_k s / Q + \omega_k^2) \quad (1)$$

where ω_k is the oscillation frequency of the targeted mode. Q is the quality factor, which is usually set to be 1. The band-pass filter is designed to concentrate the control energy only at the targeted mode and reduce its impact on other modes.

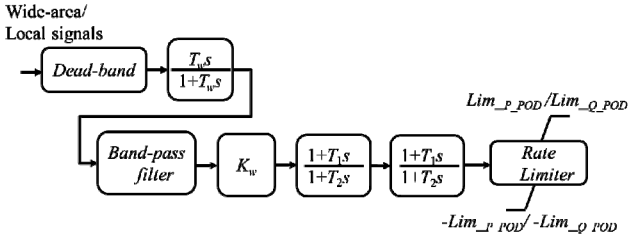

Figure 2. POD structure at IBRs

III. POD DESIGN APPROACH

The flowchart of the proposed POD design method to mitigate low-frequency oscillations is shown in Fig. 3. The targeted oscillation modes are determined first through small signal analysis results. The LFOs with damping ratio lower than 10% will be selected as the targeted ones to be damped by PODs. Fast Fourier Transform (FFT) algorithm will be used to compare the energy of all candidate PMU measurements at the targeted oscillation frequency under different events. For each targeted oscillation mode, the ones with high FFT magnitude will be selected as the optimal wide-area observation signals for wide-area POD. Local POD will adopt the local bus frequency deviation as the feedback signal. Residues of the control loop at each targeted oscillation mode represent its production of controllability and observability of the mode, and can also be used to calculate the POD parameters. Since the wide-area observation signals have been selected, the controllability of each actuator can be reflected by the residue magnitude. To reduce the impact on other modes, the IBRs with the larger residue magnitude at the targeted mode but smaller residue magnitude at the other modes will be selected as the optimal wide-area POD actuators. Similarly, the IBRs with the higher residue magnitude at the targeted mode of its local control loop will be selected as the optimal local POD actuators. If more than two modes have similar residue magnitude and frequency, then the residue angles of different modes will be checked for each control loop. To avoid any negative impact on the other oscillation modes, only the loop that have the residue angles of the different modes within the same phase and less than 90-degree difference are selected.

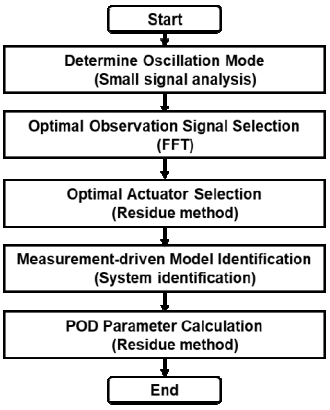

Figure 3. Design procedure of POD through IBRs

A simplified measurement-driven model of the control loop will be constructed to calculate the parameters of PODs for each control loop. Detailed algorithms are given below.

A. *Measurement-driven Model Identificaiton*

Phase compensator (T_1 and T_2) and gain (K_w) are the critical parameters to determine the POD performance. When modulating active/reactive power of IBRs, residue method can be used to obtain the compensation phase and gain based on the transfer function of the power system model. To construct the transfer function of the control loop, a probing signal is added to *Paux* or *pfaref* under a normal operating condition. Output error (OE) model structure (2) is adopted in this study for the measurement-driven model. The prediction error method (PEM) [14] is used to identify the parameters of (2) with the collected observation signal response as output and the probing signal as input.

$$y(t) = G(z^{-1})u(t) + e(t) \tag{2}$$

where $y(t)$ is the observation signal response and $u(t)$ are probing signal, $e(t)$ is the error, $G(z^{-1})$ is

$$G(z^{-1}) = \frac{z^{-n_k}(b_1 + b_2 z^{-1} + \cdots + b_{n_b} z^{-n_b+1})}{1 + f_1 z^{-1} + \cdots + f_{n_f} z^{-n_f}} \tag{3}$$

Here the probing signal is filtered white noise signal, which can concentrate its energies in the dominant mode frequency range. The measurement-driven model can update in real-time and reflect the dynamic oscillation properties of the entire system. The POD controller parameters are then tuned based on the residue of measurement-driven model to guarantee its online damping performance.

B. *POD Parameter Determination*

The identified discrete OE model can always be transformed as the continuous model and be represented as a sum of partial fractions of the form

$$G(s) = \sum_{k=1}^{n} \frac{R_k}{s - \lambda_k} \tag{4}$$

where R_k is the residue associated with the mode λ_k.

The compensation angle and gain of POD can be calculated with the residue method

$$\angle K(j\omega_k) + \angle R_k = 180^\circ \tag{5}$$

and the amplitude satisfies

$$\left|K(j\omega_k)\right| \cdot \left|R_k\right| = \left|-(\xi_t - \xi_k)\omega_k\right| \tag{6}$$

where ω_k and ξ_k are the oscillation frequency (rad/s) and damping ratio of the targeted inter-area oscillation mode. ξ_t is the targeted damping ratio, which is usually set to be 15%.

The parameters of POD can be calculated with the following equations [13]:

$$\begin{cases} \alpha = (1+\sin\theta_{\max})/(1-\sin\theta_{\max}),\ \theta_{\max} = \angle \boldsymbol{K}(j\omega_k)/2 \\ \boldsymbol{T}_1 = \alpha \boldsymbol{T}_2, \boldsymbol{T}_2 = 1/(\sqrt{\alpha}\omega_d) \\ \boldsymbol{K}_w = \left|\boldsymbol{K}(j\omega_k)\right| \Big/ \left(\left|(1+\boldsymbol{T}_1 s)/(1+\boldsymbol{T}_2 s)\right|_{s=j\omega_d}\right)^2 \end{cases} \tag{7}$$

IV. CASE STUDY ON TEXAS POWER GRID

A. *Texas Power Grid Model and Oscillation Mode Analysis*

The 2000-bus synthetic Texas power grid model is used in this project. The model was built from publicly available information by Texas A&M University [15]. As shown in Fig. 4, the system has eight areas. The red arrows indicate the power flow directions among these areas. There is a large amount of power transfer from Area 7 (Coast) and Area 8 (East) to Area 5 (North Central). To facilitate the optimal actuator selection, IBRs with large capacity are preselected as the candidate POD actuators.

Two dominant oscillation modes are identified in this model through a small-signal analysis tool - DSAtools/SSAT. One is between Area 4 and Area 7, whose oscillation frequency is 0.67 Hz, and the damping ratio is 5.10%. While, Area 1, 2, 3, 4, 5, and west part of Area 8 also oscillate against Area 7 and east part of Area 8 as another mode, whose oscillation frequency is 0.60 Hz, and the damping ratio is 6.31%.

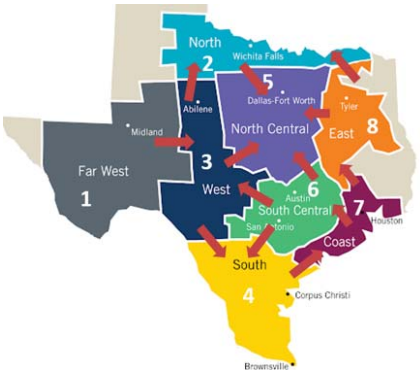

Figure 4. Texas power grid diagram

B. *Observation Signal and Actuator Selection*

For wide-area PODs, FFT and residue method are used to select its observation signal and actuator selection respectively. Three-phase fault events at different locations are used to excite both Mode 1 and Mode 2. For each case, the normalized FFT results of each measurement signal at the oscillation frequencies of the two modes are ranked from high to low. The measurement signals with the largest FFT magnitudes at frequencies of the two modes are selected separately. In this study, the frequency difference between Bus 4192 in Area 4 and Bus 7076 in Area (f_{4192}- f_{7076}) with the maximum FFT magnitude for both Mode 1 and Mode 2 is selected as the optimal observation signal for wide-area PODs at IBRs.

The residue magnitude of each IBR in different areas are also compared, and the IBRs with the largest residues at one mode while having the smallest magnitude at the other one is selected as the wide-area POD actuators. In this way, both modes can be suppressed with minimum impact on each other. In this study, IBR at Bus 4153 in Area 4 with the highest residue magnitude at Mode 1 and lowest residue magnitude at Mode 2 is selected to control Mode 1. IBR at Bus 7422 in Area 7 with the highest residue magnitude at Mode 2 and lowest residue magnitude at Mode 1 is selected to control Mode 2.

Different from wide-area PODs, local PODs adopt the local bus frequency as their feedback signal. For each candidate local IBR actuator, the one with the largest residue magnitude at one mode while having the smallest residue magnitude at the other one is selected as the local POD actuator. IBR at Bus 4153 in Area 4 with the highest residue magnitude at Mode 1 and lowest residue magnitude at Mode 2 is selected to control Mode 1 with local POD. IBR at Bus 8077 in Area 8 with the highest residue magnitude at Mode 2 and lowest residue magnitude at Mode 1 is selected to control Mode 2.

The observation signals and actuators for both wide-area POD and local POD are summarized in Table I.

TABLE I. OBSERVATION SIGNAL AND ACTUATOR SELECTION RESULTS

POD type	Observation signal		Actuator	
	Mode 1	Mode 2	Mode 1	Mode 2
Wide-area	f_{4192}-f_{7076}	f_{4192}-f_{7076}	IBR at Bus 4153 in Area 4	IBR at Bus 7422 in Area 7
Local	Local bus frequency	Local bus frequency	IBR at Bus 4153 in Area 4	IBR at Bus 8077 in Area 8

C. POD Control Design

The probing input signal with 10Hz sampling rate is added to *Paux* or *pfaref* of the selected actuator in Table I. The corresponding observation signal with 10Hz sampling rate is collected as the output for identifying model (3). The parameters of the PODs are calculated according to the residue method introduced in Section III.B. Table II lists the parameters of the wide-area POD controllers by modulating the active power of IBRs at Bus 4153 and Bus 7422. The active power modulation amplitude is limited within ±10%.

Similar to PODs with active power modulation of IBRs, Table III lists the parameters of the wide-area POD controllers by modulating the reactive power of IBRs at Bus 4153 and Bus 7422. The reactive power modulation maximum amplitude is set to be $Lim\_{Q\_WADC}=atan(Qmax/Pelec)$. *Qmax* is the limit for reactive power regulator of the electrical control model REECCU1, and the *Pelec* is the electrical power output of the IBR.

Table IV and Table V list the parameters of the local POD controllers by modulating the active or reactive power of IBRs at Bus 4153 and Bus 8077.

TABLE II. PARAMETERS OF WIDE-AREA PODS THROUGH P MODULATION OF IBR

IBR Bus	K_w	T_1	T_2	Lim $_{P\_POD}$	ω_k
4153	145	0.2375	0.2375	0.1	4.21
7422	-281	0.2806	0.2275	0.1	3.96

TABLE III. PARAMETERS OF WIDE-AREA PODS THROUGH Q MODULATION OF IBR

IBR Bus	K_w	T_1	T_2	Lim $_{Q\_POD}$	ω_k
4153	-2041	0.2083	0.2709	0.5693	4.21
7422	8000	0.2255	0.2830	0.9601	3.96

TABLE IV. PARAMETERS OF LOCAL PODS THROUGH P MODULATION OF IBR

IBR Bus	K_w	T_1	T_2	Lim $_{P\_POD}$	ω_k
4153	-196	0.2375	0.2375	0.1	4.21
8077	-308	0.2526	0.2526	0.1	3.96

TABLE V. PARAMETERS OF LOCAL PODS THROUGH Q MODULATION OF IBR

IBR Bus	K_w	T_1	T_2	Lim $_{Q\_POD}$	ω_k
4153	4290	0.1823	0.3096	0.5693	4.21
8077	8100	0.1819	0.3509	0.9601	3.96

D. POD Performance Comparison

To validate the POD damping performance on both Mode 1 and Mode 2, Event 1 in Area 4 (three-phase temporary fault at Line 4040-4079) which can excite Mode 1 and Event 2 in Area 8 (three-phase temporary fault at Line 8030-8158) which can excite both Mode 1 and 2 are simulated with different types of PODs.

1) Comparison of IBR PODs through active and reactive power modulation: Fig. 5 (a) and (b) show the bus frequency in Area 4 without and with wide-area IBR POD control under the two different events. Both Mode 1 and Mode 2 can be damped through wide-area IBR POD control with active and reactive power modulation. Compared with reactive power modulation, active power modulation is more effective to support the system recovery to the steady state. Similar to the wide-area IBR POD, the local IBR POD through active power modulation is more effective than reactive power modulation to support the system recovery to the steady state. Due to space limitation, detailed comparisons are summarized in Columns 3 and 4 of Table VI.

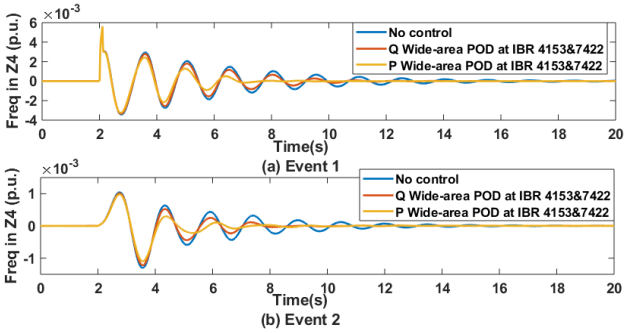

Figure 5. Wide-area IBR POD performance comparison between P and Q modulation

2) Comparison of local and wide-area IBR PODs: Fig. 6 (a) and (b) show the bus frequency in Area 4 with local or wide-area IBR POD control through active power modulation under the two different events. Compared with local feedback signal, wide-area IBR POD control has a slightly better damping performance on Mode 2. For the POD control through reactive power modulation, similar phenomena can be observed. Due to the page limitation, detailed comparison can be found between Column 4 and 6 in Table VI.

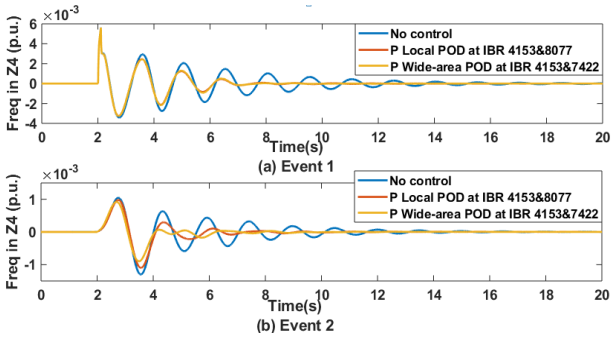

Figure 6. Wide-area and local IBR POD control performance comparison through active power modulation

3) Comparison of wide-area PODs via IBR and synchronous generator: To compare the wide-area POD performance via synchronous generator and IBR, the synchronous generator at Bus 4030 with the highest magnitude at Mode 1 is selected to control Mode 1. The generator at Bus 7208 with the highest residue magnitude at Mode 2 is selected to control Mode 2. Here the control command of wide-area PODs through synchronous generators is added to the voltage reference of Automatic Voltage Regulation (AVR). Fig. 7 (a) and (b) show the bus frequency in Area 4 with wide-area POD through

synchronous generators and wide-area IBR POD control through active/reactive power modulation under the two different events. Compared with wide-area PODs through synchronous generators, wide-area IBR POD control through active power modulation is more effective than POD through synchronous generator. Wide-area IBR POD control through reactive power modulation has similar damping performance as wide-area PODs through synchronous generators.

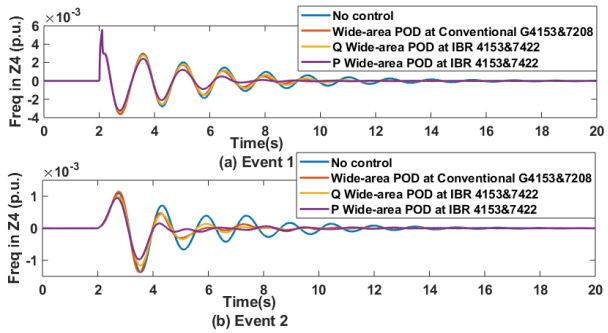

Figure 7. Performance comparison between wide-area POD control through IBR and synchronous generator

The POD performance on damping Mode 1 and Mode 2 for all cases is listed in Table VI. Compared with POD through synchronous generator, both wide-area and local IBR POD control through active power modulation are more effective than wide-area POD through synchronous generators. Both wide-area and local IBR PODs through reactive power modulation have similar damping performance with wide-area PODs at synchronous generators.

TABLE VI. DAMPING PERFORMANCE OF DIFFERENT TYPES OF PODS

POD Type	Actuator	Mode 1		Mode 2	
		Freq. (Hz)	Damp. (%)	Freq. (Hz)	Damp. (%)
No POD	N/A	0.670	6.22	0.630	8.70
Local POD via P	IBR at 4153 & 8077	0.726	12.71	0.610	>20
Local POD via Q	IBR at 4153 & 8077	0.706	8.00	0.613	15.32
Wide-area POD via P	IBR at 4153 & 7422	0.702	15.00	0.600	>20
Wide-area POD via Q	IBR at 4153 &7422	0.712	9.64	0.596	17.09
Wide-area POD via AVR	Synchronous Generator at 4030 & 7208	0.689	10.36	0.595	18.08

V. SUMMARY

Wide-area and local POD controllers at IBRs are designed in a synthetic Texas power grid model using a measurement-driven transfer function model. The POD performance is validated to improve the small-signal stability by dynamic simulations. Based on the simulation results, either active or reactive power modulation of IBRs with wide-area and local POD can suppress the two dominant oscillations effectively. PODs through active power modulation of IBRs are more effective than reactive power modulation of IBRs in suppressing the LFOs. Compared with local PODs, wide-area PODs have slightly better damping performance. Local PODs with good controllability of the targeted inter-area mode can be a backup when remote wide-area signals are unavailable. Additionally, compared to wide-area PODs at synchronous generators, PODs through active power modulation of IBRs can damp the oscillations more quickly. PODs through reactive power modulation of IBRs can achieve similar damping performance as wide-area PODs at synchronous generators. The PODs at IBRs can support the small-signal stability of power systems with high renewable penetration. Considering the power grid variations with high renewable penetration, adaptive POD design for different power system operating conditions will be studied in the future.

REFERENCES

[1] W. Yao, L. Jiang, J. Wen, Q. H. Wu, and S. Chen, "Wide-area damping controller of FACTS devices for inter-area oscillations considering communication time delay," *IEEE Trans. Power Syst.,* vol. 29, pp. 318-329, Jan. 2014.

[2] Z. Obaid, L.M. Cipcigan, and Mazin T. Muhssin, "Power system oscillations and control: Classifications and PSSs' design methods: A review," *Renewable and Sustain. Energy Reviews*, vol. 79, pp. 839-849, Nov. 2017.

[3] S. Eftekharnejad, V. Vittal, G.T. Heydt, B. Keel, and J. Loehr, "Impact of increased penetration of photovoltaic generation on power systems," *IEEE Trans. Power Syst.,* vol. 28, pp. 893-901, May. 2013.

[4] C. Liu, G. Cai, W. Ge, D. Yang, C. Liu, and Z. Sun, "Oscillation analysis and wide-area damping control of DFIGs for renewable energy power systems using line modal potential energy," *IEEE Trans. Power Syst.*, vol. 33, no. 3, pp. 3460-3471, May 2018.

[5] L. L. Fan, H. P. Yin, and Z. X. Miao, "On active/reactive power modulation of DFIG-based wind generation for interarea oscillation damping," *IEEE Trans. Energy Convers.*, vol. 26, no. 2, pp. 513-521, Jun. 2011.

[6] J. C, Neely, R. H. Byrne, R. T. Elliott, C. A. Silva-Monroy, D. A. Schoenwald, D. J. Trudnowski, et al, ""Damping of Inter-area Oscillations using Energy Storage," in *Proceedings of IEEE PES General Meeting*, Vancouver, BC, Canada, 2013, pp. 1-5.

[7] Y. Hashmy, Z. Yu, D. Shi, and Y. Weng, "Wide-Area Measurement System-Based Low Frequency Oscillation Damping Control Through Reinforcement Learning," *IEEE Trans. Smart Grid*, vol. 11, no. 6, pp. 5072-5083, Nov. 2020.

[8] Y. Zhao, C. Lu, P. Li, and L. Tu, "Applications of wide-area adaptive HVDC and generator damping control in Chinese power grids," in *Proceedings of IEEE PES General Meeting*, Boston, MA, USA, 2016, pp. 1-5.

[9] C. Liu, G. Cai, W. Ge, D. Yang, C. Liu and Z. Sun, "Oscillation analysis and wide-area damping control of DFIGs for renewable energy power systems using line modal potential energy," *IEEE Trans Power Syst*, vol. 33, no. 3, pp. 3460-3471, May 2018.

[10] M. Saadatmand, G. B. Gharehpetian, A. Moghassemi, J. M. Guerrero, P. Siano and H. H. Alhelou, "Damping of Low-Frequency Oscillations in Power Systems by Large-Scale PV Farms: A Comprehensive Review of Control Methods," *IEEE Access*, vol. 9, pp.72183-72206, 2021.

[11] Western Electricity Coordinating Council, "WECC Solar PV Dynamic Model Specification," Salt Lake City, UT, September 2012.

[12] Y. Zhao, C. Lu, J. Yong, and Y. Han, "Residue and identification based wide-area damping controller design in large-scale power system," *in Proc. IEEE PES Conference on Innovative Smart Grid Technologies,* Washington. DC, USA, Jan. 2012.

[13] J. Zhang, C. Y. Chung, and Y. Han, "A novel modal decomposition control and its application to PSS design for damping inter-area oscillations in power systems," *IEEE Trans. Power Syst.*, vol. 27, pp. 2015-2025, Nov. 2012.

[14] Ljung L. "System Identification: Theory for the User," *Prentice Hall PTR*, 1999.

[15] ACTIVSg2000: 2000-bus synthetic grid on footprint of Texas. [Online]. Available: https://electricgrids.engr.tamu.edu/electric-grid-test-cases/activsg2000/.